EUROPHYSICS LETTERS 15 April 2005

*Europhys. Lett.*, **70** (2), pp. 237–243 (2005)
DOI: 10.1209/epl/i2004-10484-x

# Quantum helimagnetism of the frustrated spin-$\frac{1}{2}$ chain $LiCuVO_4$

M. Enderle[1], C. Mukherjee[2], B. Fåk[3], R. K. Kremer[4], J.-M. Broto[5], H. Rosner[6], S.-L. Drechsler[7], J. Richter[8], J. Malek[7,9], A. Prokofiev[10], W. Assmus[10], S. Pujol[1], J.-L. Raggazzoni[1], H. Rakoto[5], M. Rheinstädter[1] and H. M. Rønnow[11]

[1] *Institut Laue-Langevin - BP 156, 38042 Grenoble Cédex 9, France*
[2] *Clarendon Laboratory - Parks Road, Oxford, OX1 3PU, UK*
[3] *DRFMC/SPSMS, CEA - 38054 Grenoble, France*
[4] *Max-Planck Institute for Solid State Research - 70569 Stuttgart, Germany*
[5] *Laboratoire National des Champs Magnétiques Pulsés - 31432 Toulouse, France*
[6] *Max-Planck Institute for Chemical Physics of Solids - 01187 Dresden, Germany*
[7] *Institut für Festkörpertheorie im IFW Dresden - Dresden, Germany*
[8] *Theoretische Physik, Universität Magdeburg - Magdeburg, Germany*
[9] *Institute of Physics, ASCR - Prague, Czech Republic*
[10] *Johann Wolfgang von Goethe Universität - Postfach 111932, 60054 Frankfurt, Germany*
[11] *Paul-Scherrer-Institut - 5232 Villigen PSI, Switzerland*

received 14 December 2004; accepted in final form 25 February 2005
published online 18 March 2005

PACS. 75.10.Jm – Quantized spin models.
PACS. 75.30.-m – Intrinsic properties of magnetically ordered materials.
PACS. 71.20.-b – Electron density of states and band structure of crystalline solids.

**Abstract.** – Inelastic neutron scattering, susceptibility, and high-field magnetization identify $LiCuVO_4$ as a nearest-neighbour ferromagnetic, next-nearest-neighbour frustrated, quasi–one-dimensional helimagnet, which is largely influenced by quantum fluctuations. Complementary band structure calculations provide a microscopic model with the correct sign and magnitude of the major exchange integrals.

Geometrically frustrated spin-$\frac{1}{2}$ systems display a rich variety of exotic ground states, reflected in gapped or gapless, discrete and/or continuous excitation spectra, and often lack a classical analogue [1]. Even in the perhaps most simple frustration model, the purely one-dimensional (1D) Heisenberg model with competing nearest, $J_1$, and next-nearest neighbour interactions, $J_2$, the ground state phase diagram is complex and remarkably different from the classical case. This model is identical to the zigzag chain with leg exchange $J_2$ and rung (zigzag) exchange $J_1$. Theoretical work has been focused on the subspace with antiferromagnetic nearest (*nn*) and next-nearest neighbour (*nnn*) interactions, where a dimerized gapped phase [2–4] is surrounded by gapless commensurate [5] and gapped incommensurate

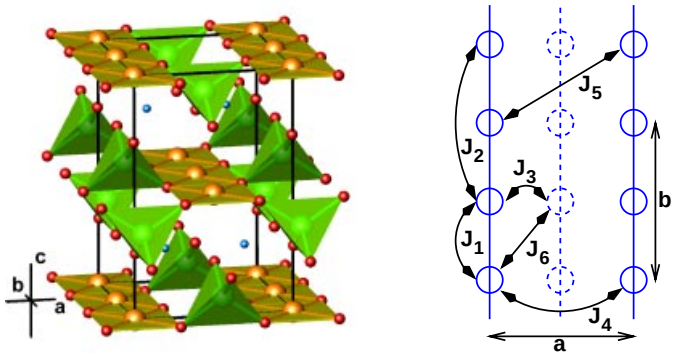


Fig. 1 – Left: crystal structure of $LiCuVO_4$. (In the on-line colour version, the $VO_4$ tetrahedra are highlighted in green, the $CuO_2$ bands in light olive). Right: scheme of exchange paths between the $Cu^{2+}$ in the $ab$-plane (solid) and to a layer shifted by $c/2$ (dashed).

phases [6–9]. Nevertheless, large quantum effects are predicted even for frustrated ferromagnetic $nn$ and antiferromagnetic $nnn$ interactions ($FM_{nn}$-$AF_{nnn}$). Bursill *et al.* [6] report that, contrary to the classical helimagnet, the pitch angles of the $FM_{nn}$-$AF_{nnn}$ quantum helimagnet remain very close to $\frac{\pi}{2}$ for a wide range of frustration ratios $J_2/J_1$.

Most of the few known quasi-1D frustrated spin-$\frac{1}{2}$ materials are discussed in terms of antiferromagnetic nearest-neighbour interaction [10–13]. The similarity of fits for the susceptibility and high-field magnetization of models with largely different frustration ratios [11], as well as striking discrepancies between proposed models and realistic exchange paths [10, 13–16], mark the difficulties and ambiguities in the determination of exchange integrals for frustrated systems.

Here we present a study on $LiCuVO_4$, first associated with a frustrated chain by Gibson *et al.* [17], on the basis of neutron diffraction and single-crystal susceptibility data. The present measurements of the dispersion in off-symmetry directions, combined with high-temperature susceptibility data and magnetization, allow a more reliable determination of the exchange integrals than low-temperature susceptibility and ordering vector alone, or susceptibility and high-field magnetization alone. The latter may give a good idea for a simple interaction scheme, but are clearly insufficient to classify materials with frustrated interactions properly. The exchange integrals extracted from the present measurements are remarkably well described by our theoretical calculations. This demonstrates that realistic microscopic models developed via band structure calculations are capable of backing up the signs and even the order of magnitude of the major exchange integrals in copper oxide materials.

$LiCuVO_4$ crystallizes in the space group *Imma* [18], with edge-shared $CuO_2$ chains running along $b$ as illustrated in fig. 1. The magnetic structure is helical with propagation vector $(0\,0.532\,0)$ [17]. Earlier susceptibility and magnetization [19, 20], specific heat [21], ESR [22–24], and NMR [25] studies have been interpreted in terms of various one- and two-dimensional models, ranging from the anisotropic $AF$ chain [23] to the square Ising lattice [21]. Our study combines inelastic neutron scattering, susceptibility, and high-field magnetization data, as well as band structure calculations and exact diagonalization studies of multi-band Hubbard and Heisenberg models. We achieve a consistent picture, which reveals $LiCuVO_4$ as the first clear example of a frustrated quasi-1D $FM_{nn}$-$AF_{nnn}$ helimagnet strongly influenced by quantum effects.

Single crystals of $LiCuVO_4$ were grown from solutions of $LiCuVO_4$ in a $LiVO_3$ or $LiVO_3$-LiCl melt [26]. The temperature-dependent susceptibility of $LiCuVO_4$ was measured with magnetic field $B||a,c$ in a MPMS7 SQUID magnetometer, the high-field magnetization with $B||a,c$ at $T = 1.7\,\mathrm{K}$ in a 60 T pulsed field at LNCMP, Toulouse.

The dispersion of the magnetic excitations was determined by inelastic neutron scattering experiments on the thermal and cold 3-axis instruments IN20 and IN12 installed at ILL. IN20 was set up with $k_f = 2.662\,\mathrm{Å}^{-1}$ and PG-filter in $k_f$. On IN12 we used $k_f = 1.55\,\mathrm{Å}^{-1}$ or $1.3\,\mathrm{Å}^{-1}$, and a 77 K-Be filter in $k_f$ to suppress higher orders. A $60\,\mathrm{mm}^3$ single crystal of $LiCuVO_4$ (the same as for the neutron diffraction measurement [17]) was aligned in the $(hk0)$, $(0k\ell)$, or $(0.05656\ell\ k\ \ell)$ plane and kept at base temperature of a helium cryostat ($T = 2\,\mathrm{K}$, IN20) or a dilution fridge ($T = 50$–$150\,\mathrm{mK}$, IN12). All data were taken in the ordered phase below $T_N = 2.1\,\mathrm{K}$, verified by the presence of a magnetic Bragg peak. For the low-energy data, the tail of the incoherent elastic scattering was determined at the nearest $b^*$ zone boundary, $k = \pm 0.23$. In order to extract the exchange integrals, the excitation energies and the incommensurate ordering vector were fitted simultaneously to a classical Heisenberg spin wave dispersion [27]. The lower boundary of the excitation spectrum of a spin-$\frac{1}{2}$ Heisenberg system is well described by a classical spin-wave dispersion relation with renormalized $AF$ exchange integrals $RJ$. In the spin wave model, we considered exchange between nearest and next-nearest neighbours along $b$, $J_1([0\frac{1}{2}0])$ and $J_2([010])$, in the $ab$-plane away from $b$, $J_4([100])$ and $J_5([1\frac{1}{2}0])$, and out of the $ab$-plane, $J_3([\frac{1}{2}0\frac{1}{2}])$ and $J_6([\frac{1}{2}\frac{1}{2}\frac{1}{2}])$, cf. fig. 1.

To obtain further insight into the electronic structure of $LiCuVO_4$, band structure calculations within the local density approximation (LDA) have been carried out using a full-potential nonorthogonal local-orbital code [28] and the exchange correlation potentials of Perdew-Wang [29]. Cu and V $(3s, 3p, 4s, 4p, 3d)$ and O and Li $(2s, 2p, 3d)$ states were chosen as the basis set. All lower-lying states were treated as core states. The inclusion of Cu and V $(3s, 3p)$ states in the valence states was necessary to account for non-negligible core-core overlaps due to the relatively large extension of the Cu and V $(3s, 3p)$ wave functions. The Li $(2p, 3d)$ and O $(3d)$ states were taken into account to get a more complete basis set. Brillouin zone integrations were done using the tetrahedron method. Convergence with respect to the basis set and the $k$-mesh was carefully checked. Applying exact diagonalization and the calculation of response functions within the continued fraction technique, an extended Hubbard model has been constructed which simulates the electronic ground-state configuration. The susceptibility has been calculated by full diagonalization of a $N = 16$ frustrated $J_1$-$J_2$ Heisenberg ring.

Inelastic neutron scattering reveals a steep dispersion of the magnetic excitations in the $b^*$ direction, and very little dispersion perpendicular to $b^*$ (fig. 2), confirming a pronounced 1D character. The zone boundary energies at $k \approx 0.23$ and $k \approx 0.73$ are clearly different, and exclude the uniform chain model [23]. Energy scans close to the two 1D zone boundaries are displayed in fig. 3. If only data taken in high-symmetry directions were considered, the intrachain dispersion and the ordering wave vector would be compatible with both an antiferromagnetic and a ferromagnetic $nn$ interaction (but with different interchain interactions). This ambiguity is lifted when taking into account the dispersion in off-symmetry directions, displayed as well in figs. 2, 3. The full data set is only compatible with ferromagnetic $nn$ intrachain interaction $J_1$, and antiferromagnetic $nnn$ interaction $J_2$. The solid and dashed lines in fig. 2 indicate our spin-wave model with $J_4 = 0$, and a model with only $J_1$, $J_2$, $J_4$, respectively. Including $J_4$ does not improve the fit (cf. table I), while any model with $J_5 = 0$ can be excluded. The renormalized exchange integrals $R_iJ_i$ obtained by the spin-wave fits are assembled in table I. The renormalization factor $R_i$ is known to be 1 for ferromagnetic interactions or parallel spin alignment, hence $R_iJ_i = J_i$ for $i = 1, 3, 5$. $R_6J_6$ is rather insignificant, thus only the renormalization of the $AF_{nnn}$ exchange $J_2$ plays a role. The uniform $AF$

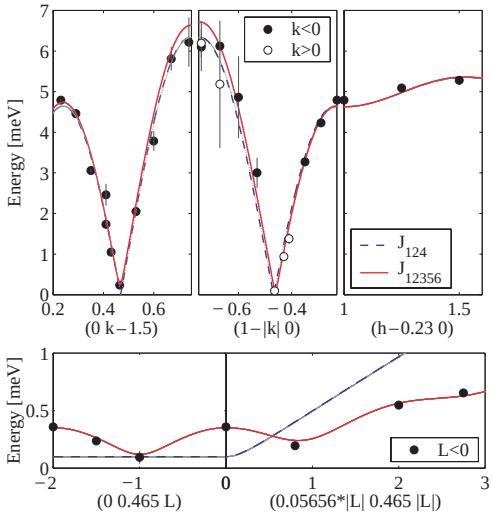


Fig. 2

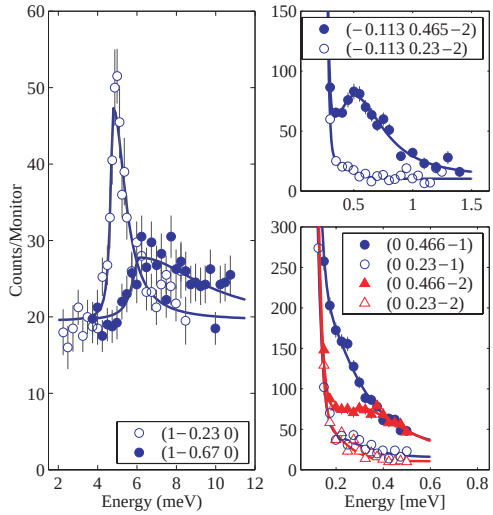


Fig. 3

Fig. 2 – Dispersion of the magnetic excitations of $LiCuVO_4$. The lines represent spin-wave fits. Solid (red in the on-line version): $J_1$, $J_2$, $J_3$, $J_5$, $J_6$ varied, $J_4 = 0$, cf. table I. Dashed (blue in the on-line version): $J_1$, $J_2$, $J_4$ varied, $J_3, J_5, J_6 = 0$.

Fig. 3 – Energy scans of $LiCuVO_4$ at different wave vectors. Left: scans close to the 1D zone boundaries, $T = 2\,\mathrm{K}$, $k_f = 2.662\,\mathrm{\AA}^{-1}$, monitor $\sim 2\,\mathrm{min}$ (IN20). Right: scans close to the 1D zone center with corresponding zone boundary scans as background estimate, $T \approx 100\,\mathrm{mK}$ (IN12). Top: $k_f = 1.55\,\mathrm{\AA}^{-1}$, monitor $\sim 10\,\mathrm{min}$. Bottom: $k_f = 1.3\,\mathrm{\AA}^{-1}$, monitor $\sim 8\,\mathrm{min}$.

spin-$\frac{1}{2}$ Heisenberg chain has $R = \frac{\pi}{2}$, and $R$ has been found experimentally close to $\frac{\pi}{2}$ even in the presence of quite sizable interchain interaction or frustration [30]. Here we determine $R_2$ by fitting $J_2$ in the high-temperature series expansion (eq. 5a in [31]) to the susceptibility, keeping all other $J_i$ constant.

The saturation field is indicated by pronounced peaks in the magnetization derivative $\mathrm{d}M/\mathrm{d}(\mu_0 H)$ at $B^a_{sat} \approx 49.7\,\mathrm{T}$ and $B^c_{sat} \approx 41\,\mathrm{T}$, shown in fig. 4. Figure 4 also displays the $B||a$ susceptibility and inverse susceptibility together with the exact diagonalization of a $N = 16$-ring and the high-temperature series expansion (eq. 5a in [31]). Our susceptibility data are consistent with earlier results, but extend to much higher temperatures. $J_1$ and $J_2$ of the 1D-ring calculation have been adapted to $\chi$. Neglecting the frustrating interchain

TABLE I – *Exchange interactions per bond extracted from the magnetic excitations and the susceptibility, together with the extended TB parameters of the band structure and Hubbard model estimates ($U = 4.25\,\mathrm{eV}$). Units are* meV, *the paths $i$ are defined in fig.* 1. *$J_i > 0$ favors AF alignment.*

| | Method | $i=1$ | 2 | 3 | 4 | 5 | 6 |
|---|---|---|---|---|---|---|---|
| $R_i J_i$ | neutron scattering | −1.6(2) | 5.59(8) | −0.014(10) | 0.01(3) | −0.40(8) | 0.08(4) |
| $R_i J_i$ | neutron scattering | −1.6(2) | 5.60(8) | −0.015(9) | – | −0.37(5) | 0.08(4) |
| $J_i$ | high-$T$ series fit to $\chi$ | −1.6 | 3.87(2) | −0.015 | – | −0.37 | 0.08 |
| $J_i$ | $N = 16$-ring fit to $\chi$ | −1.8 | 4.3 | – | – | – | – |
| $J_i$ | LDA/TB | −3 | 6.1 | 0.11 | 0.79 | 0.06 | 0.02 |
| $t_i$ | LDA/TB | −74 | −83 | 11 | 29 | 8 | −5 |

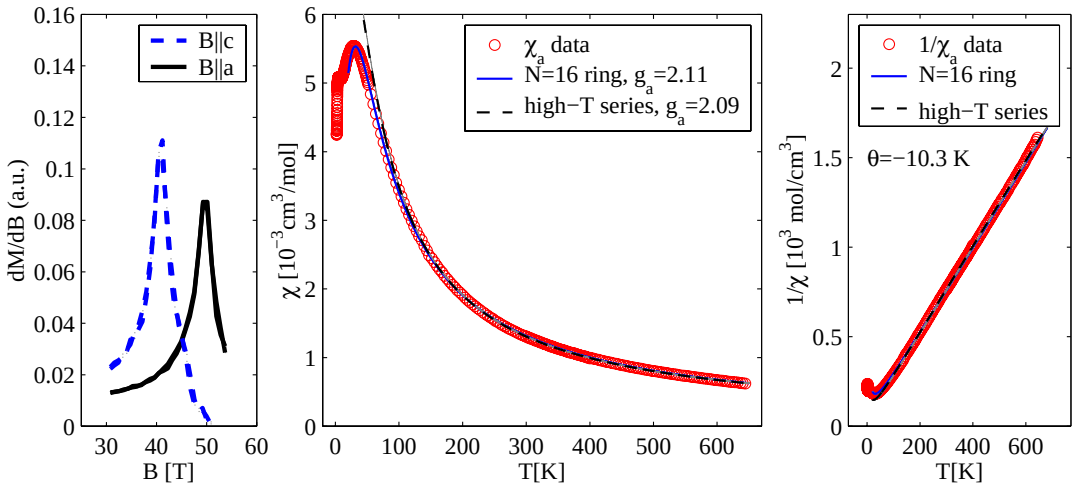


Fig. 4 – Left: derivative of the magnetization of $LiCuVO_4$ *vs.* field, $B||a, c$. The large peaks indicate the saturation field. Middle: susceptibility $\chi_a$. Right: inverse susceptibility $1/\chi_a$, in comparison with the high-temperature series expansion and the $N = 16$-ring calculation, cf. table I.

interactions leads to slightly compromised values of $J_1$ and $J_2$. Nevertheless, the overall agreement is remarkable. For the high-temperature series expansion, we used $g_a = 2.09$, close to the value determined by ESR, $g_a = 2.07$ [23], and the exchange integrals from inelastic neutron scattering ($J_4 = 0$, table I), with $R_2 = 1.45$, very close to $\frac{\pi}{2}$. The same parameter set predicts the saturation fields $B^a_{sat} = 48.1\,\mathrm{T}$ and $B^c_{sat} = 43.5\,\mathrm{T}$ ($g_c = 2.313$ [23]). The high-temperature series expansion describes the susceptibility very well above 170 K; above 250 K, the susceptibility approaches within 1% a Curie-Weiss law with $k_B\theta = \sum_i J_i(\vec{r}_i)/2$.

The calculated band structure as well as the total and partial density of states (DOS) are shown in fig. 5. Our calculations result in non-magnetic $V^{5+}$ and magnetic $Cu^{2+}$ sites in agreement with an empirical argumentation based on the crystal structure. The valence band has a width of about 7 eV typical for cuprates, and predominantly Cu $3d$ and O $2p$ character. We find two well-isolated narrow bands at the Fermi level (fig. 5, left panel) corresponding to the Cu $4a$-sites. These antibonding bands show dominant Cu $3d$ - O $2p$ character. The V and Li contributions are negligible. A more detailed orbital analysis reveals that only the Cu $3d_{xy}$ and the chain O $2p_{x,y}$ states contribute significantly. Therefore, the mapping of our LDA results to an effective one-band tight-binding (TB) model, and the subsequent construction of single-band Hubbard and extended Heisenberg models should reflect the low-energy properties in good approximation. A corresponding TB model has been derived and fitted to the LDA band structure of fig. 5 along the high-symmetry lines. The resulting main transfer integrals $t_i$ (notation analogous to the exchange paths in fig. 1) are given in table I. The related $AF$ superexchange integrals $J_i^{AF} = 4t_i^2/U$ [32] show a pronounced quasi-1D behaviour. Ferromagnetic contributions $J_i^{FM}$ play a role for the short-range terms, only. In analogy to $Li_2CuO_2$ and $CuGeO_3$ [33], we generated $J_1$ and $J_2$ from Coulomb matrix elements using bare one-band Wannier functions and an additional exponential screening with a screening length of 4 Å. The resulting effective exchange integrals $J_i$ are given in table I. Our microscopic model yields the correct sign and within a factor of 2 even the size of the intrachain interactions, contrary to Dai *et al.* [34]. Within our microscopic model, $J_3$, $J_4$, $J_5$,

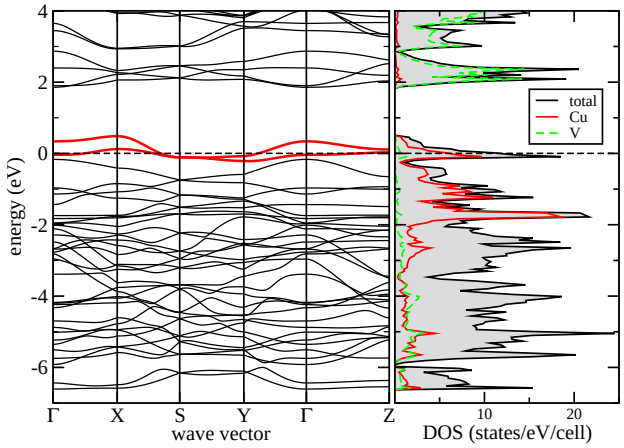


Fig. 5 – Band structure (left panel), total and partial density of states (right panel) for $LiCuVO_4$. The Fermi level is at zero energy. The notation of the symmetry points is as follows: X($\frac{1}{2}$00), S($\frac{1}{2}\frac{1}{2}$0), Y(0$\frac{1}{2}$0), Z(001) in reciprocal lattice units. The Cu bands relevant for the low-energy TB model are indicated by thicker (red in the on-line version) lines.

$J_6$ are small compared to $J_1$ and $J_2$, in agreement with the experiment. The experimentally observed ferromagnetic sign of $J_5$ can be understood qualitatively from Hund's rule coupling at the O $2p_{x,y}$ orbitals (not taken into account in the calculation) overcompensating the weak $AF$ superexchange contribution.

The experimentally observed incommensurability translates into a pitch angle of $83.6 \pm 0.6°$. Pitch angle and frustration ratio, $\alpha = J_2/(J_1+2J_5-4J_6) = -1.43$, can be compared with the classical and quantum 1D predictions. For the frustration ratio $\alpha$ as found in $LiCuVO_4$, the classical prediction yields $\arccos(-1/(4\alpha)) = 79.9°$, a much smaller pitch angle than the quantum 1D model [6], which predicts 88° for $J_2/J_1 = -1.43$. Obviously, the quantum fluctuations in $LiCuVO_4$ tend to keep the pitch angle closer to 90° than the classical prediction, but are less developed than one would expect from the 1D theory. One might speculate that interchain interactions suppress in part the quantum fluctuations. However, the even larger interchain interactions in the 2D frustrated $Cs_2CuCl_4$ do not affect the quantum fluctuations visibly: the quasi-1D $AF$ exchange is renormalized by a similar factor $R \approx \frac{\pi}{2}$ as in the purely 1D $AF$ chain [30]. Another potential influence are anisotropies: ESR detected a 6% anisotropy [23]. While there are no calculations available for the $FM_{nn}$-$AF_{nnn}$ case, for $AF_{nn}$-$AF_{nnn}$ interactions, the anisotropy needs to be very large to influence the pitch angle visibly, and tends to drive it closer to 90° rather than towards the classical pitch angle [35]. Finally, impurities would rather drive the system to a shorter ordering period than a longer one, hence would tend to keep the pitch angle closer to 90° rather than driving it to smaller values. Hence, the reason for the considerable deviation from Bursill's prediction remains unclear.

To summarize, our results demonstrate that $LiCuVO_4$ can be described coherently with a frustrated $FM_{nn}$-$AF_{nnn}$ chain model supplemented with a small ferromagnetic frustrating interchain interaction. With the large antiferromagnetic $nnn$ interaction $J_2$ renormalized by $R = 1.45$ in the classical spin wave dispersion, the exchange integrals determined by neutron scattering consistently explain the susceptibility and the saturation magnetization. The large renormalization factor demonstrates the dominance of quantum fluctuations, also expressed by the tendency of the quantum helimagnet to keep the pitch angle closer to $\frac{\pi}{2}$ than expected from the classical prediction.

* * *

Financial support by the DFG, SPP 1073 (SLD, JM) and the Emmy-Noether Program (HR) is gratefully acknowledged. For the full Heisenberg diagonalization JR used J. Schulenburg's *spinpack*.

REFERENCES

[1] Richter J. *et al.*, *Lect. Notes Phys.*, **645** (2004) 85.
[2] Majumdar C. K. and Ghosh D. K., *J. Math. Phys.*, **10** (1969) 1388; 1399.
[3] Shastry B. S. and Sutherland B., *Phys. Rev. Lett.*, **47** (1981) 964.
[4] Haldane F. D. M., *Phys. Rev. B*, **25** (1982) 4925.
[5] Okamoto K. and Nomura K., *Phys. Lett. A*, **169** (1992) 433.
[6] Bursill R. *et al.*, *J. Phys. Condens. Matter*, **7** (1995) 8605.
[7] Chitra R. *et al.*, *Phys. Rev. B*, **52** (1995) 6581.
[8] White S. R. and Affleck I., *Phys. Rev. B*, **54** (1996) 9862.
[9] Tonegawa T. and Harada I., *J. Phys. Soc. Jpn.*, **56** (1987) 2153.
[10] Masuda T. *et al.*, *Phys. Rev. Lett.*, **92** (2004) 177201.
[11] Maeshima N. *et al.*, *J. Phys. Condens. Matter*, **15** (2003) 3607.
[12] Kikuchi H. *et al.*, *Physica B*, **284-288** (2000) 1631.
[13] Boehm M. *et al.*, *Europhys. Lett.*, **43** (1998) 77.
[14] Mizuno Y. *et al.*, *Phys. Rev. B*, **60** (1999) 6230.
[15] de Graaf C. *et al.*, *Phys. Rev. B*, **66** (2002) 14448.
[16] Gippius A. A. *et al.*, *Phys. Rev. B*, **70** (2004) 20406.
[17] Gibson B. J. *et al.*, *Physica B*, **350** (2004) e253.
[18] Lafontaine M. A. *et al.*, *Acta Cryst.*, **C45** (1989) 1205.
[19] González C. *et al.*, *J. Mat. Sci.*, **29** (1994) 3458.
[20] Vasil'ev A. N., *JETP Lett.*, **69** (1999) 876.
[21] Yamaguchi M. *et al.*, *J. Phys. Soc. Jpn.*, **65** (1996) 2998.
[22] Vasil'ev A. N. *et al.*, *Phys. Rev. B*, **64** (2001) 24419.
[23] Krug von Nidda H.-A. *et al.*, *Phys. Rev. B*, **65** (2002) 134445.
[24] Kegler C. *et al.*, *Eur. Phys. J. B*, **22** (2001) 321.
[25] Tanaka T. *et al.*, *J. Phys. Soc. Jpn.*, **71** (2002) 308.
[26] Prokofiev A. V. *et al.*, *J. Cryst. Growth*, **220** (2000) 345.
[27] Nagamiya T., *Solid State Physics*, edited by Seitz F. *et al.*, Vol. **20** (Academic Press, New York) 1967, p. 305.
[28] Koepernik K. and Eschrig H., *Phys. Rev. B*, **59** (1999) 1743.
[29] Perdew J. P. and Wang Y., *Phys. Rev. B*, **45** (1992) 13244.
[30] Coldea R. *et al.*, *Phys. Rev. Lett.*, **88** (2002) 127203.
[31] Johnston D. C. *et al.*, *Phys. Rev. B*, **61** (2000) 9558.
[32] A value of $U = 4.25\,\mathrm{eV}$ has been adopted in analogy to the five-band extended Hubbard model analysis of the optical conductivity and XAS data for related $CuO_2$ chains compounds.
[33] Rosner H. *et al.*, *Physica B*, **259-261** (1999) 1001.
[34] Dai D. *et al.*, *Inorg. Chem.*, **43** (2004) 4026.
[35] Aligia A. A. *et al.*, *Phys. Rev. B*, **62** (2000) 3259.